Dual-Step Reduction of Copper and Formation Mechanism of Cu Pseudo-Icosahedral Microcrystals

Weihao Sun and Wuzong Zhou*

Read Online

ACCESS | Metrics & More | Article Recommendations | Supporting Information

ABSTRACT: Pseudo-icosahedral Cu microcrystals have been synthesized in a solvothermal system containing $CuSO_4 \cdot 5H_2O$ as the precursor, polyvinylpyrrolidone (PVP) as a reductant/capping agent, and dimethylformamide as the solvent. The structural and morphological evolutions over the reaction time are investigated, which enable us to establish a novel formation mechanism of pseudo-icosahedral crystals of Cu. The first crystalline phase that appeared in the solution is $Cu_4SO_4(OH)_6 \cdot H_2O$ in the form of microflakes. The microflakes are reduced and decomposed to Cu_2O nanocrystallites, which assemble with PVP into spherulites. The Cu_2O crystals are further reduced to Cu nanocrystallites, which aggregate with PVP again into spherical particles. An extraordinary phenomenon is that 20 separated (111) triangular plates form on each particle during surface recrystallization of Cu, and their locations match to the final facets of the pseudo-icosahedron. The plates extend to cover the whole surface of the sphere, forming a pseudo-icosahedral shell, followed by extension of the recrystallization from the surface to the core. This reversed crystal growth process increases the thickness of the plates until all the Cu nanocrystallites in the core are consumed. It is found that, during the surface recrystallization of polycrystalline spheres, the particles preferentially select the (111) planes of the face-centered cubic structure of Cu as the exposed faces because these planes have the minimum surface binding energy. The particles then try to keep as small as possible the specific surface area, and a pseudo-icosahedral shape consisting of 20 (111) plates, which has a specific surface area, about 10% lower than that of an octahedron, formed by eight (111) plates. Accordingly, the overall surface free energy of a pseudo-icosahedron is about 10% lower than that of an octahedron. The formation of tetrahedra as building units of icosahedra, as predicted previously, has not been observed. The formation of ideal icosahedra, the so-called perfect Platonic solid, and the formation of twin defects between neighboring (111) plates are not possible. The newly proposed formation mechanism of pseudo-icosahedra Cu sheds light on the understanding of formation of many other polyhedral crystals.
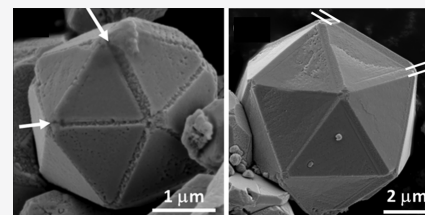
1. INTRODUCTION

Formation of polyhedral morphologies of crystals has been investigated over one century. The most common crystal growth route starts with a nucleus followed by repeated attachment of the building units. According to the Bravais−Friedel−Donnay−Harker (BFDH) law[1−3] and the Hartman−Perdok theory,[4] the crystal growth rate varies with the crystallographic orientation and is proportional to the surface attachment energy, which is inversely proportional to the interplanar d-spacing along a specific direction.[5] During the crystal growth, the faces on the fast growing directions would grow out and the final morphology would be a polyhedron with the facets along the slowest growing orientations. For example, if face-centered cubic (fcc) crystals have the largest d-spacing between the adjacent (111) planes, then the normal morphology would be octahedral consisting of eight identical (111) facets.

On the other hand, unlike the kinetic approach of the BFDH law above, Curie and Wulff believed that a crystal morphology intended to maintain the minimum surface free energy,[6,7] considering that the crystal growth rate was not essential. Surface free energy on a crystal facet is the energy needed to split the crystal parallel to this face defined by Miller indices

(hkl). Although Curie−Wulff's theorem is also applied to explain formation of polyhedral morphologies of crystals, the polyhedra consisting of a single type of facet, such as a cube, octahedron, etc., often do not meet the requirement of minimum specific surface free energy. The truncated polyhedra, e.g., truncated cube and truncated octahedron, normally can further reduce the specific surface free energy. Consequently, the actually observed crystal morphologies are often the results from a balance between kinetic and thermodynamic factors.

Many crystal growth routes are much more complicated and cannot be elucidated by either the BFDH law or Curie−Wulff's theorem. For example, when $AgNO_3$ was reduced by polyvinylpyrrolidone (PVP) in N,N-dimethylformamide (DMF), both decahedral and icosahedral Ag metal crystals

could be produced.[8] It was proposed that the formation mechanisms of these morphologies were due to the step-by-step assembly of 5 or 20 pre-formed tetrahedra. Unfortunately, solid evidence of such intelligent assembly was not obtained. In particular, the chance to form icosahedra by perfect aligning of 20 tetrahedra is extremely small.

Tsuji *et al.* proposed a stepwise growth of silver tetrahedral units, forming multiple twin planes on the (111) faces. In other words, a tetrahedron forms first. The second tetrahedron grows on the first tetrahedron by sharing a (111) plane to form a twin defect,[9] followed by attachment of the third tetrahedron, and so on.

In theory, the so-called icosahedron of metal formed by 20 tetrahedra will not be a perfect Platonic solid, which is constructed by congruent, regular, and polygonal faces with the same number of faces meeting at each vertex. As shown in Figure 1, the projected angle between two adjacent ridges in an
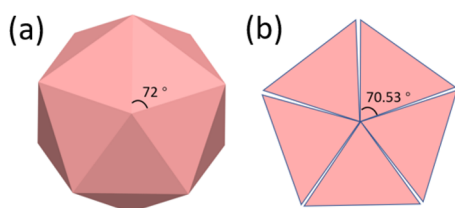

Figure 1. (a) Ideal icosahedron (Platonic solid) viewed along one vertex with a projected angle of 72° between the adjacent ridges. (b) Projection of a pseudo-icosahedron formed by five tetrahedra with the interplanar angle of the adjacent (111) faces parallel to the view direction, 70.53°.

ideal icosahedron is 72°, while the corresponding angle in the particle formed by 20 tetrahedra, *i.e.*, the angle between two adjacent (111) planes, is 70.53°. An average mismatch between the tetrahedra is 1.47°. Therefore, the stepwise intergrowth of tetrahedra via twin defects would not lead to an ideal icosahedral morphology. It was realized that the icosahedra of silver could only exist when the particle size was small,[9] in which the lattice tension at the boundaries could be released by surface relaxation.

In addition to silver crystals, the icosahedral nanoparticles of gold[10,11] and copper[12] can also be produced. The formation mechanisms of these metallic nanocrystals should be similar. It was stated that, in weak reducing conditions, stepwise growth might be preferred, while in strong reducing conditions, twined nuclei might form and classical growth would lead to big icosahedra.[10] However, such metallic icosahedra obtained from solvothermal methods all stay in the nanoscale. The annealing process and chemical vapor deposition can produce microscale icosahedral crystals,[13−15] while the angular mismatch aforementioned always exists, which may be overcome by filling in extra atoms in the gaps between the adjacent tetrahedra. Consequently, due to the inevitable angular mismatch, all these polyhedra formed by 20 (111) facets are not Platonic solids but can be called pseudo-icosahedra.

Herein, we report the synthesis of pseudo-icosahedral Cu microcrystals via a solvothermal method using $CuSO_4$ as the precursor, DMF as the solvent, and PVP as the surfactant and mild reductant. Based on microstructural investigations of the specimens at different crystal growth stages, a new formation mechanism is revealed. The pseudo-icosahedral Cu microcrystals do not form from assembly of tetrahedra but are constructed by 20 (111) plates due to surface recrystallization

of polycrystalline spheres followed by a process of reversed crystal growth.

2. EXPERIMENTAL SECTION

2.1. Materials. $CuSO_4 \cdot 5H_2O$ (Sigma-Aldrich), polyvinylpyrrolidone (PVP, Sigma, mol wt 360,000), dimethylformamide (DMF, Acros Organics, 99+%), and deionized water with a resistivity of 18.3 $M\Omega$ cm^{-1} were used without further purification.

2.2. Synthesis of Cu Crystals. The specimens were synthesized using previously established methods for Ag polyhedral crystals[8,9] with several modified conditions. The use of Cu sulfate was decided after testing some common salts, such as $CuCl_2$, $Cu(NO_3)_2$, $Cu(CH_3COO)_2$, $Cu(SO_4)$, *etc.* Only sulfate gave a large amount of pseudo-icosahedral Cu microcrystals. Selection of reductants was also performed using NaH_2PO_2, $NaBH_4$, ascorbic acid, PVP, *etc.* Only PVP was suitable for producing pseudo-icosahedral Cu microcrystals. In a typical synthesis, 0.5 g of PVP was fully dissolved in 25 mL of DMF and pre-heated to 150 °C before adding 1.25 mmol of $CuSO_4 \cdot 5H_2O$. The solution was stirred continuously until it became a green suspension. The suspension was then transferred into an autoclave vessel and was heated in an oven at 150 °C for 12 h. Reaction time was then varied to obtain samples from different growth stages. When the reaction was stopped, the sample was filtered and washed three times with water to remove residual SO_4^{2-}, DMF and PVP remained. Finally, the obtained powder was dried at 50 °C. All experiments were performed three times to make sure they were repeatable.

2.3. Specimen Characterization. Powder X-ray diffraction (XRD) was performed on a STOE diffractometer in Debye−Scherrer (capillary) mode in room temperature using Cu $K_{\alpha1}$ ($\lambda = 1.5405$ Å) radiation. The inner diameter of the capillary was 0.5 mm. The diffracted X-rays were collected using a scintillation position-sensitive linear detector. The scanning range was from 10 to 80°, and the scanning time was 12 h for each XRD pattern. Scanning electron microscopy (SEM) images were recorded using JEOL IT-200 and IT-800 microscopes operated from 5 to 15 kV. Samples were coated with gold for overcoming the beam charge problem. Energy-dispersive X-ray spectroscopy (EDS) data were collected by the integrated EDS detectors at 20 kV. EDS samples were deposited on silica substrates, instead of carbon tape, without a gold coating to avoid the impurity carbon and gold. Soft X-ray emission spectra (SXES) were collected on an SEM IT-800 microscope using an SXES detector at −70 °C with a collection time of 1 h for each spectrum. Fourier transform infrared spectroscopy (FTIR) data was collected using a Shimadzu IRAffinity-1s spectrometer. Transmission electron microscopy (TEM) and high-resolution TEM (HRTEM) images were obtained using two microscopes: JEOL JEM 2011 and FEI Titan Themis 200S/TEM (in TEM mode) both operated at 200 kV. Samples for TEM observation were dispersed in acetone or ethanol and deposited onto a TEM specimen grid supported by a holey carbon film.

3. RESULTS AND DISCUSSION

In the synthetic solution containing $CuSO_4$, PVP, and DMF, Cu^{2+} cations were gradually reduced in two steps to form Cu crystals. After the reaction for 12 h, a large amount of Cu pseudo-icosahedral microparticles (1−4 μm in diameter) was obtained, as shown in Figure 2. The particle morphology is similar to an ideal Platonic icosahedron, as seen in the inset of Figure 2b, which has 30 edges and 20 equilateral triangular faces with 5 of them meeting at each of the 12 vertices.

To reveal the microstructural changes and morphology evolution over reaction time, the reaction was stopped at 1.5, 2, 3, 6, 9, and 12 h. Characterization was performed on each specimen.

Powder XRD patterns of the specimens at different reaction times were obtained (Figure 3). The pattern of the 1.5 h sample shows two phases. The peaks of the main phase are indexed to monoclinic $Cu_4SO_4(OH)_6 \cdot H_2O$ and space group
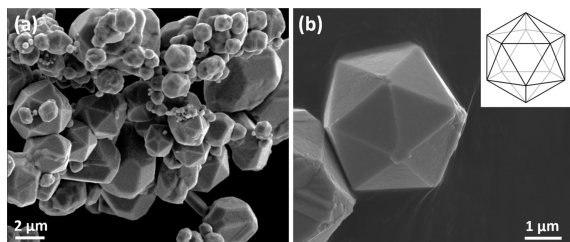
Figure 2. (a) SEM image of the Cu pseudo-icosahedral crystals after reaction for 12 h. (b) SEM image of a single pseudo-icosahedron. The inset shows the geometry of an ideal Platonic icosahedron.
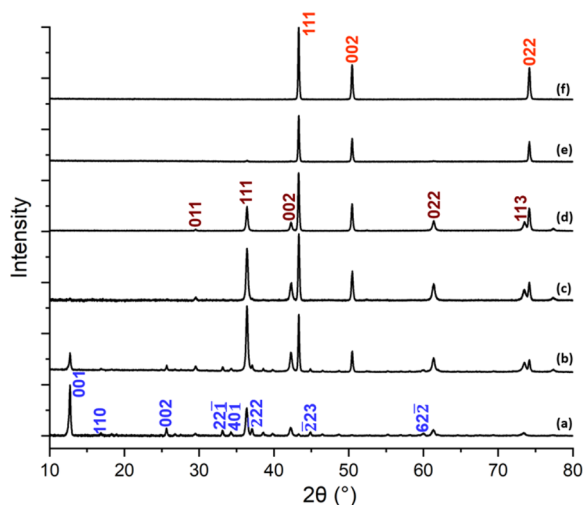

Figure 3. Powder XRD patterns of specimens prepared with different reaction times of (a) 1.5, (b) 2, (c) 3, (d) 6, (e) 9, and (f) 12 h. Three phases are identified, and their patterns are indexed to (a) monoclinic $Cu_4SO_4(OH)_6 \cdot H_2O$, (d) cubic Cu_2O, and (f) face-centered cubic Cu.

P_a, with the unit cell parameters of $a = 10.578$, $b = 6.345$, $c = 7.863$ Å, and $\beta = 117.98°$ (ICSD Code-100276). Its corresponding mineral is named posnjakite, which shows a greenish blue color and rhombus habit. Therefore, it is also regarded as a pseudo-hexagonal structure. The second phase is cubic Cu_2O with the unit cell parameter $a = 4.268$ Å (ICSD Code-67850), as indexed on pattern (d) in Figure 3. The color appearance of the samples supports the XRD results (Figure S1). In 10 min, the solution turned to a green suspension, which is the color of $Cu_4SO_4(OH)_6 \cdot H_2O$. The 1.5 h sample shows a gray purple color, resulting from the mixed phases of $Cu_4SO_4(OH)_6 \cdot H_2O$ (greenish blue) and Cu_2O (dark brown).

The powder XRD results indicate that Cu^{2+} formed $Cu_4SO_4(OH)_6 \cdot H_2O$ crystals initially with the oxidation state of Cu unchanged and was gradually reduced by PVP to form Cu_2O. Commercially available PVP normally contains hydroxyl groups due to the existence of H_2O and H_2O_2 in its industry production process of polymerization. Figure S2 shows the monomer of PVP and the structures of hydrogen-terminated and hydroxyl-terminated PVP. PVP can serve as a dispersant to prevent inorganic nanoparticles from aggregation.[16,17] On the other hand, nanoparticles capped by PVP can agglomerate into large composite particles due to strong inter-molecular interaction of PVP. Hydroxyl-terminated PVP also shows a mild reducing ability to reduce metal cations.[17−20]

When the reaction time was increased to 2 h, the XRD peak intensities of $Cu_4SO_4(OH)_6 \cdot H_2O$ decreased, while those of Cu_2O increased (Figure 3). The color of the specimen became

darker (Figure S1c), indicating a big decrease in the ratio of $Cu_4SO_4(OH)_6 \cdot H_2O$ to Cu_2O. The Cu phase also emerged at this stage, which is face-centered cubic with the unit cell parameter $a = 3.615$ Å. No peaks of $Cu_4SO_4(OH)_6 \cdot H_2O$ are shown in the XRD pattern of the 3 h sample or any later samples. The middle stage of the reaction was the stage when Cu_2O and Cu co-existed. Meanwhile, the peaks of Cu_2O became weaker and those of Cu got stronger as the reaction time increased. The color of the specimens gradually changes from deep brown to reddish brown, implying the transformation from Cu_2O to Cu (Figure S1). In the XRD pattern of the 9 h sample, only a small bump of Cu_2O (111) is seen. In the 12 h sample, Cu_2O seems to completely disappear, leaving a pure Cu phase in the DMF solution. The reddish brown color of 9 and 12 h samples is typical for Cu metal.

The morphology and size of the produced crystals were observed from SEM and TEM images. Crystal structures of the specimens were determined by using HRTEM images. The SEM and TEM images of $Cu_4SO_4(OH)_6 \cdot H_2O$ from the 1.5 h sample show that the crystals exhibit thin microflakes (Figure S3c), which reflects the crystal structure consisting of relatively stable $Cu_4(OH)_6^{2+}$ layers parallel to the (ab) plane and connected by SO_4^{2-} anions via hydrogen bonds along the c axis (Figure S3a). Consequently, the growth rate of extension of the (ab) plane is much faster than that along the c axis. The typical shape of the microflakes is a rhombus plate. The obtuse angle of this rhombus plate is measured to be $\gamma = 121°$, which matches the obtuse angle of a pseudo-hexagonal unit cell (Figure S3b). The crystals were beam-sensitive, and HRTEM images of the intact structure were not recorded. Further characterization of the thin flakes by EDS confirmed that the crystals contained Cu, S, and O (Figure S4a).

The second phase in the 1.5 h sample presents as spherical particles, ~5 μm in diameter, as shown in Figure 4a. These spheres have a grainy surface. The images of the cross section of the spheres show a spherulite construction (Figure 4b) with needle-like particles lying down along the radial directions. A similar structure was found in naturally occurring and biomimetic synthesized calcite spherulites, in which the needle-like particles contained orientated calcite nanocrystallites embedded in an alginate polymer substrate.[21] The self-orientated assembly of calcite nanocrystallites was due to their dipolar property. In the present work, HRTEM images also detected orientated Cu_2O nanocrystallites (<5 nm in diameter) embedded in a polymer matrix, as shown in Figure 4c, implying that the nanocrystallites of Cu_2O may generate a dipolar field when their two opposite surfaces terminate at the Cu^+ and O^{2-} layers. The corresponding fast Fourier transform (FFT) pattern looks like a single-crystal diffraction pattern (inset of Figure 4c). The d-spacings measured from the image confirm the Cu_2O structure.

The EDS spectrum from a spherulite shows characteristic X-rays from Cu, O, and C (Figure S4b). Oxygen comes from Cu_2O and PVP, and carbon is merely from PVP. N in PVP was not detected by EDS due to its small content and severe absorption of its X-rays. Nevertheless, N was detected by other techniques as discussed below.

In addition to the microflakes and spherulites, a lot of separated nanocrystallites were also detected from the TEM images of 1.5 and 2 h samples (Figure S5). Similar nanoparticles were found in other samples with the reaction time from 2 to 6 h. These nanocrystallites are mainly Cu_2O as confirmed by further investigation below, and it is believed that
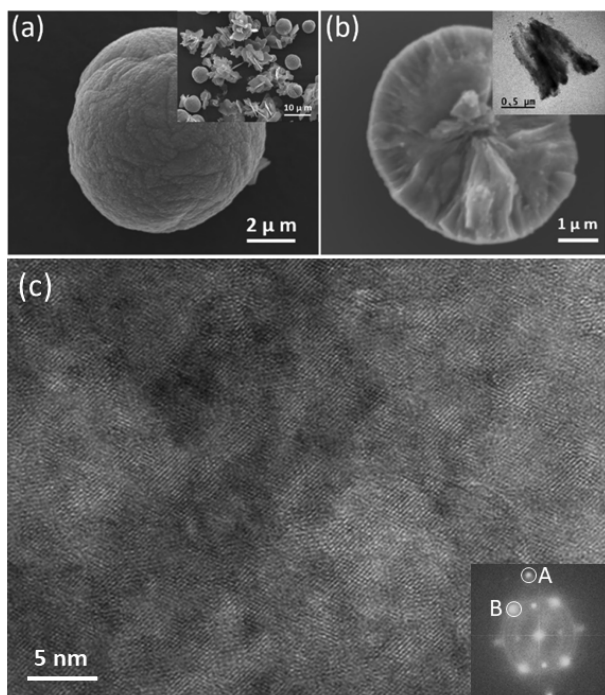
Figure 4. (a) SEM image of a spherical particle in a 1.5 h specimen. The inset is a low magnification SEM image showing the co-existence of $Cu_4SO_4(OH)_6 \cdot H_2O$ microflakes and Cu_2O-containing spheres. (b) SEM image of a cross section of a sphere, revealing a spherulite structure consisting of needle-shaped particles lying down along the radial directions. The inset shows a fragment of a few needle-like components. (c) HRTEM image from a spherulite. The inset is the corresponding FFT pattern. The d-spacings of A and B are measured 1.51 and 2.47 Å, respectively, which are indexed to the (220) and (111) planes of the cubic Cu_2O.

they came from the reduction and decomposition of the $Cu_4SO_4(OH)_6 \cdot H_2O$ microflakes. The Cu_2O nanocrystallites were capped by PVP as the building units for the spherulites.

To further confirm the existence of PVP in spherulites, FTIR was used to characterize the chemical bonds in the samples and SXES was used to detect light elements. The FTIR spectrum of the 2 h sample shows many absorption bands from PVP (Figure S6a). The relatively sharp absorption band at 3668 cm^{-1} belongs to OH stretching in the hydroxyl terminal groups of PVP. The bands of CH_2 and CH stretching (2970, 2900, 1394, and 893 cm^{-1}) are assigned to the CH_2 groups in the PVP chain. The band at 1250 cm^{-1} is related to the C−N bending vibration from the pyrrolidone structure in PVP. In addition, an absorption band is observed at 600 cm^{-1}, which is due to the vibrational mode of the Cu_2O nanostructure.[22,23] In comparison with the FTIR spectrum of pure PVP (Figure S6b), the intensity of the band of the C−O stretching (1066 cm^{-1}) significantly increases, but the intensity of the C=O stretching (1647 cm^{-1}) almost disappears. These changes can be attributed to the combination of PVP with metal cations, similar to the FTIR results of Ag/PVP.[24] Therefore, this is the evidence of capping of PVP on Cu_2O and Cu nanocrystallites. The SXES spectrum from a spherulite in the 1.5 h sample confirms C, N, and O elements in the particle. C and N are from PVP, while O is from both Cu_2O and PVP (Figure S6c).

As we discussed above, the crystal growth process of Cu can be divided into early, middle, and late stages based on the powder XRD patterns in Figure 3, which indicate several phase

transformations, accompanying with the dual-step reduction of copper from Cu^{2+} to Cu^+ and finally to Cu. In the early stage (before 2 h), the flakes of $Cu_4SO_4(OH)_6 \cdot H_2O$ appeared as the first crystalline phase, which was gradually reduced and decomposed into Cu_2O nanocrystallites. The nanocrystallites aggregated with PVP to form Cu_2O/PVP composite spherulites.

In the middle stage (2−6 h), $Cu_4SO_4(OH)_6 \cdot H_2O$ was mostly consumed. The surface of Cu_2O/PVP spherulites quickly became rough with many irregular polyhedral crystals, as shown by typical SEM images in Figure S7a,b. The EDS spectrum from the rough surface (Figure S7e) shows peaks of Cu and O, implying that the major phase of surface crystals is still Cu_2O. As seen in Figure S7c, the needle-like component in the inner structure of these rough surface particles confirms that these rough surface particles were developed from Cu_2O/PVP spherulites *via* a further surface crystal growth of Cu_2O. The wrapped Cu_2O nanocrystal-containing cores of the particles would undergo reduction and recrystallization into polyhedral Cu particles, leading to a yolk−shell structure (Figure S7d).

Also in the middle stage, many dispersed nanoparticles were observed on the carbon film of the TEM specimen grids. The HRTEM image (Figure 5a) shows that these nanoparticles are not monophasic. The d-spacings measured from Figure 5b indicate that the diffraction spots at the circles of A, B, and F can be indexed to the $(\bar{1}12)$, (211), and (014) planes of $Cu_4SO_4(OH)_6 \cdot H_2O$, respectively. Those at the circles of C, D, and G can be indexed to the (111), (200), and (221) planes of Cu_2O, respectively. E can be indexed to the (111) planes of Cu. These dispersed nanoparticles were not observed in 9 and 12 h samples. The above results imply that the nanocrystallites resulted from reduction and decomposition of the $Cu_4SO_4(OH)_6 \cdot H_2O$ microflakes. In other words, the micro-flakes were gradually reduced and split into Cu_2O nanocrystals, some of which were further reduced to Cu nanocrystals. A small number of $Cu_4SO_4(OH)_6 \cdot H_2O$ nanocrystallites were the unreacted fragments of the microflakes. Later on, the $Cu_4SO_4(OH)_6 \cdot H_2O$ nanocrystallites would also be reduced to Cu_2O. The Cu_2O nanocrystallites would act as the building units of spherulites, while the Cu nanocrystallites would aggregate into spherical particles with a smooth surface.

The irregular polyhedral particles on the rough surface spheres would be also reduced and decomposed to Cu nanocrystallites. Figure S8a,b shows corroded Cu_2O polyhedral crystals, and the original smooth surface of these crystals becomes porous. The result of this corrosion was the formation of Cu nanocrystallites (Figure S8c). With the help of the capping molecules, these nanocrystallites aggregated into Cu/PVP composite spherical particles with different sizes. These spherical particles were different from the Cu_2O spherulites, and the Cu nanocrystallites randomly located in the particles without forming needle-like nanorods, in which the nanocrystallites were self-orientated. Their surface was relatively smooth without further development into irregular polyhedral crystals. On the other hand, the surface recrystallization did happen, forming a crystalline shell (Figure S9).

In the synthesis of zeolite analcime, nanocrystallites aggregated into large spheres. The surface of these spheres then recrystallized into a thin icositetrahedral single-crystalline shell consisting of 24 identical {211} facets followed by extension of the recrystallization from the surface to the core,[25]
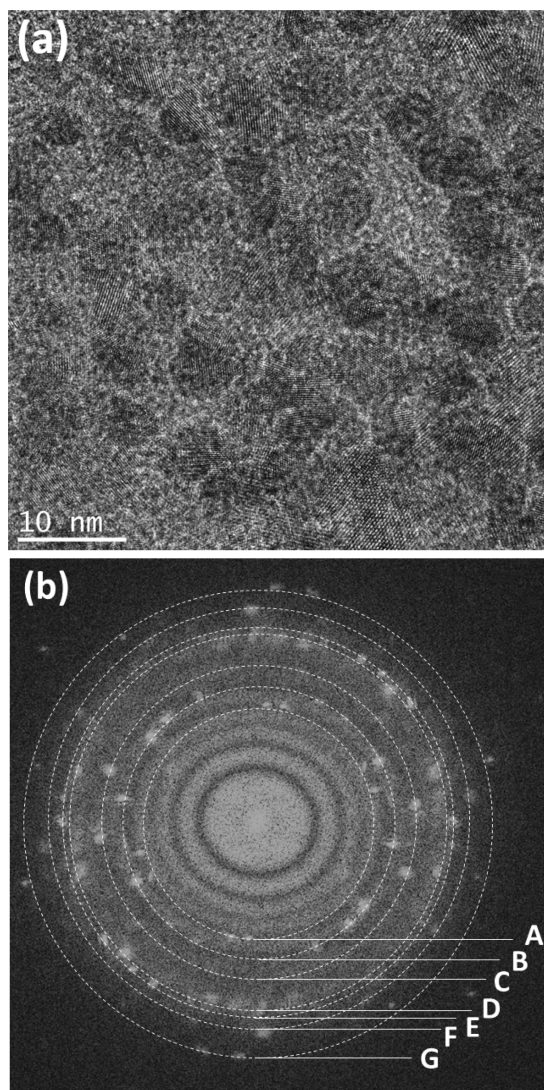
Figure 5. (a) HRTEM image from the 6 h sample, showing separated nanocrystallites. (b) Corresponding FFT pattern. The *d*-spacings of the rings measured are A: 3.34 Å, B: 2.89 Å, C: 2.51 Å, D: 2.11 Å, E: 2.00 Å, F: 1.67 Å, and G: 1.43 Å.

Figure 6. SEM images showing surface recrystallization of the polycrystalline Cu/PVP spheres. (a) Some triangular plates are developed at the surface of a small sphere from the 6 h sample. (b) Particle from the 9 h sample, showing almost complete 20 triangular plates, which are still separated with a narrow gap, indicated by the arrows. (c) Broken icosahedral particle from the 9 h sample, showing increased thickness (∼300 nm) of the surface plates. (d) TEM image of a triangular plate found in a crushed 9 h sample. The inset is the corresponding SAED pattern, showing the [111] view direction of the fcc Cu structure.

which was the so-called reversed crystal growth. A similar process in zeolite A led to a cubic single-crystalline shell with an amorphous core.[26] When the precursor materials in the cores were completely consumed, the particles became hollow single crystals. The reversed crystal growth has been also found in metal oxides, carbonates, metal−organic frameworks, organic crystals, *etc*.[27] In fact, the formation of polycrystalline or non-crystalline aggregates is the first and crucial step of the reversed crystal growth mechanism. A similar phenomenon was observed in the present work.

The Cu/PVP spherical particles did not stay long in the system, and their surface soon underwent recrystallization into some triangular plates no matter if the size of the spheres is large or small. Figure 6a shows a small spherical particle with about 500 nm in diameter. On its surface, the Cu nanocrystallites recrystallize into a triangular plate (marked 1). The other two plates (marked 2 and 3) also start to form. They locate next to plate 1 but do not connect each other. These triangular plates developed independently on the particle surface. However, their locations seem to match
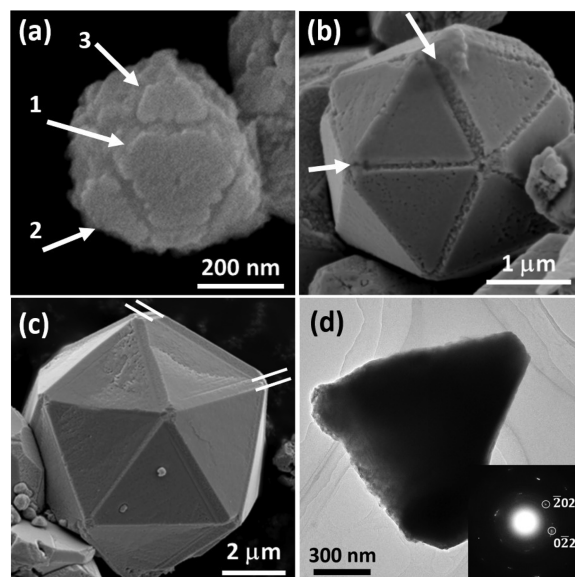
exactly the sites of the facets of an icosahedron. Up to 20 triangular plates may develop simultaneously at their own locations without direct connection. The particle in Figure 6b is an almost complete icosahedron. The triangular plates are approaching each other but are still separated with a narrow gap. From these gaps, we can see that the plates are very thin and the material underneath still contains nanocrystallites. The driving force for such a perfect self-organization of the locations of the triangular plates still remains elusive.

When the particles were crushed, some individual plates dropped down from the particles. The TEM image in Figure 6d shows a single-triangular plate. The corresponding SAED pattern shows that the plate is a single crystal. The face of the plate is the (111) plane of the Cu structure. HRTEM images directly recorded from the pseudo-icosahedral particle also confirmed the Cu structure (Figure S10c).

The triangular plates join together, completely covering the surface of the particles, although the (111) twin planes were never achieved due to the mismatching with 1.47° at each edge. The recrystallization then extends from the surface to the core. Consequently, we can see that the thickness of the surface plates increases with a longer reaction time (Figure 6c and Figure S10a) until all the nanocrystallites in the core are consumed via Ostwald ripening. Eventually, the product contains hollow pseudo-icosahedral particles (Figure S10b).

A large number of pseudo-icosahedral particles were observed in the 12 h sample. FTIR and EDS have been used to examine whether these particles are pure copper or not. Same as the FTIR spectrum of the 2 h sample (Figure S6a), in the FTIR spectrum of the 12 h sample, CH_2, CH, CN, and C−O bands are observed and assigned to PVP (Figure S11a). The results imply the existence of PVP in the cores of the particles.
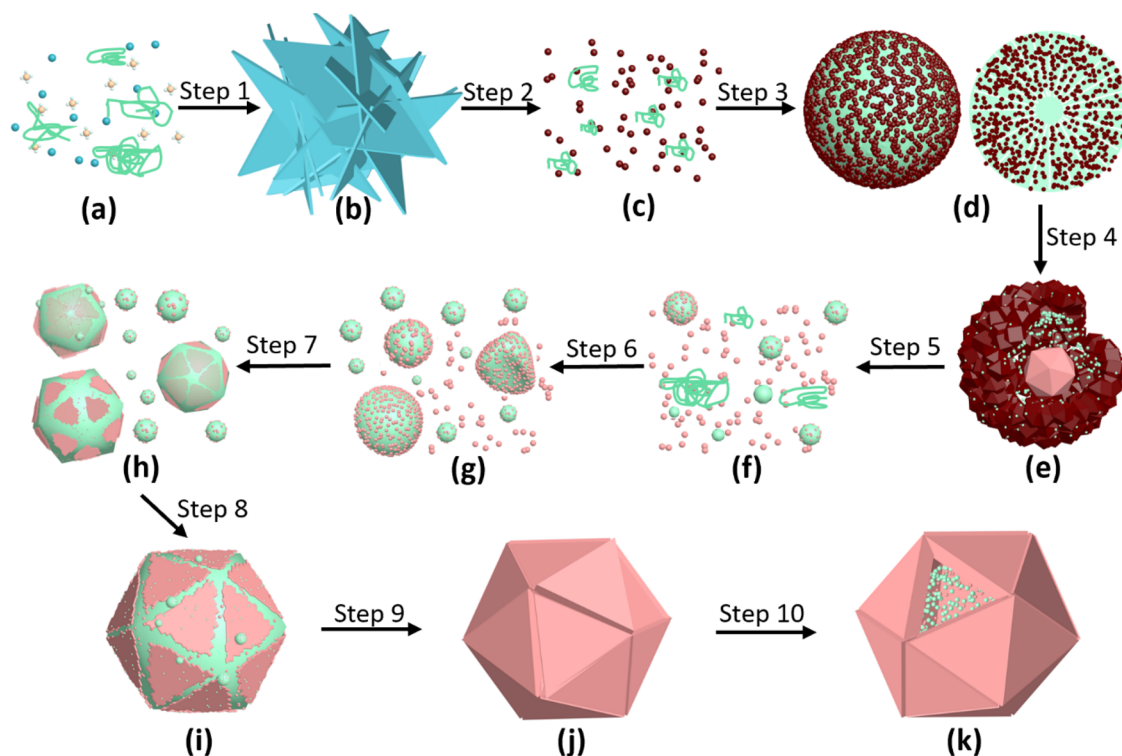
Figure 7. Schematic diagram of the proposed reduction process of copper and the formation mechanism of Cu pseudo-icosahedra. (a) Cu^{2+} (blue), SO_4^{2-} (light brown), and PVP molecules (light green) in a DMF solution. (b) $Cu_4SO_4(OH)_6 \cdot H_2O$ microflakes. (c) Cu_2O nanocrystallites (dark brown) from decomposition of the microflakes. (d) Cu_2O/PVP spherulites. (e) Cu_2O/PVP spherulite with irregular Cu_2O crystals on the surface. A Cu pseudo-icosahedron in the interior is developed, forming a yolk−shell structure. (f) Cu nanocrystallites resulted from decomposition of the Cu_2O crystals. (g) Cu/PVP aggregate into spheres. (h) Surface recrystallization to form triangular (111) plates of Cu. (i) The recrystallization extends on the particle surface to form 20 triangular (111) plates. (j) Cu pseudo-icosahedron with a narrow gap in between the adjacent (111) plates. (k) Extension of recrystallization from the surface to core of the particle, leading to thicker plates.

On the other hand, the Cu−O band is not observed in the spectrum, indicating that all Cu_2O crystallites have been reduced to Cu. The EDS spectrum (Figure S11b) from a pseudo-icosahedron shows the major element of Cu, accompanied with very low peaks of C and O. The reason for low intensities of C and O is that these elements are in the PVP molecules in the core, which are covered by the Cu plates. The penetration depth of electrons in EDS is much lower than that of IR radiation. The X-rays of the light elements in a low yield further suffer from a large absorption.

Based on the experimental results as presented above, we are able to propose phase transformations and a formation mechanism of Cu pseudo-icosahedral microparticles step-by-step (Figure 7). The dual function of PVP and a balanced kinetic and thermodynamic control in crystal growth are also discussed.

Initially, $CuSO_4 \cdot 5H_2O$ and PVP were dissolved in a DMF solution. Rhombus-shaped microflakes of $Cu_4SO_4(OH)_6 \cdot H_2O$ appeared (step 1).

As the reaction kept going, the microflakes were broken down into nanoscale fragments when Cu^{2+} cations in the microflakes were gradually reduced by the mild reducing agent PVP to form Cu_2O nanocrystallites (step 2).

In step 3, the Cu_2O nanocrystallites capped with PVP aggregated into microspherulites. A possible driving force of self-orientation of Cu_2O nanocrystallites along radial directions in the spherulites would be a dipolar field generated in the nanocrystallites.

The Cu_2O nanocrystallites near the surface of the spherulites underwent further growth to form larger irregular polyhedral Cu_2O crystals, leading to a rough surface (step 4). No large area smooth surface was observed. A similar morphology of rough surface Cu_2O hollow particles was recently reported.[28] For those spherulites, the mass transportation between the outside and the interior was restricted, thus generating a gap between the low density core and the high density shell to form a yolk−shell structure. In the core, the existing PVP gradually reduced Cu_2O nanocrystallites into Cu nanocrystallites followed by a surface recrystallization to form a pseudo-icosahedral morphology. A similar process reappeared in the morphology evolution of the Cu/PVP spheres in the solution, as demonstrated below.

On the other hand, the Cu_2O irregular crystals were further reduced by the mild reducing agent PVP in the solution and decomposed into Cu nanocrystallites (step 5). PVP then served merely as the surfactant, functioning as the agglomerating agent. Cu nanocrystallites capped by PVP subsequently assembled to form spherical particles with different sizes (step 6).

Like the typical reversed crystal growth routes,[27] crystal growth of the Cu nanocrystallites in the core of particles was suppressed due to the limited space and blocked mass transportation. The active sites for crystal growth were at the surface of the particles. In fact, 20 triangular (111) plates of the fcc Cu structure were developed on the particle surface and their locations matched the final facets of an icosahedron (step 7). Selection of the (111) planes as the exposed faces can be

explained according to Curie and Wulff's theorem[6,7] because the (111) planes have the largest d-spacing and, therefore, the minimum binding energy in the Cu crystals, ensuring that the particles can achieve a minimum local surface free energy. On the other hand, the kinetic effect on the crystal growth leads to a slow growth along the [111] direction and fast growth of the directions perpendicular to [111]. Furthermore, the reduction of the surface energy by the formation of the (111) plates on a spherical particle must associate with the cost of a small increase in the specific surface area.

These thin plates were separated and seemed to have no connection to each other. However, their locations at the beginning matched to the facets of an icosahedron. This phenomenon was observed several times in our previous work. For example, six separated crystalline plates developed on the surface of calcite polycrystalline spheres, and their locations matched perfectly a rhombohedral single-crystal shell.[29] The driving force for such an unusual manner of crystal growth has not been well understood. A possible reason could be that the nanocrystallites in the particles were well orientated, which guided the crystal orientations of the surface plates, leading to a single-crystalline shell. However, 20 (111) plates in a pseudo-icosahedron of Cu in the present work cannot form a single-crystalline shell and there are even no real twin boundaries between the facets. The harmonious formation of such plates is even more peculiar.

These (111) plates extended on the particle surface via an Ostwald ripening process, approaching to a pseudo-icosahedral morphology (step 8). At each boundary of the adjacent (111) plates, there was still a gap. When the (111) plates covered the whole surface of a particle, a pseudo-icosahedral Cu was achieved when the inter-plate boundaries were as narrow as the nanoscale (step 9). As we can imagine, the pseudo-icosahedral morphology was only a construction of 20 very thin triangular plates. The core material was still the polycrystalline Cu/PVP composite.

The recrystallization further extended from the particle surface to the core. The (111) plates therefore increased their thickness until all the Cu nanocrystallites in the core were consumed, more likely leaving a hole in the center (step 10).

If a Cu crystal grows via a classical growth route, i.e., starting with a single nucleus, followed by layer-by-layer deposition of Cu atoms without twin defects, then an octahedral morphology may be achieved with eight {111} facets.[30] This process will not lead to an icosahedron because the total number of the {111} faces in a single crystal is 8. If the crystal growth starts from a nucleus containing several twin defects, then a pseudo-icosahedral particle consisting of 20 tetrahedra may form only when the particle size is in the nanoscale. In this case, the lattice tension at the boundaries between adjacent tetrahedra may be eased by surface relaxation. It is very hard to form Cu icosahedra in the micrometer scale.[31,32] It is interesting to find in the present work that Cu particles tend to form a morphology with a minimum surface free energy by two approaches. First, the particles would develop the (111) facets because the (111) planes have the largest d-spacing and, therefore, the lowest surface binding energy (E_b) or minimum surface free energy per unit of area, (E_f). Second, the overall morphology tended to possess a minimum specific surface area. There are three possible polyhedra formed only by the (111) facets, the tetrahedron, octahedron, and icosahedron. All of them have the same E_b but different specific surface areas, A_s. The total surface free energy $E_{tot} = E_f \times A_s$. The specific

surface area of an icosahedron is about 90% of that of an octahedron and about 71% of that of a tetrahedron. Therefore, the total specific surface free energy of an icosahedron is much lower. Although there are thick boundaries between the facets, the defect area is very small. Therefore, the small rebound of surface free energy due to the defect edges of pseudo-icosahedra can be ignored. More importantly, the pseudo-icosahedral particle size can cover a wide range, from several hundred nanometers to several micrometers in diameter.

4. CONCLUSIONS

Although it is difficult to synthesize microscale icosahedral Cu crystals via the classical crystal growth route, Cu pseudo-icosahedra, a few micrometers in diameter, have been successfully synthesized in a solvothermal system by using mild reducing agent PVP. However, the particles are not formed by 20 tetrahedral components and there are no true twin defects. The pseudo-icosahedral morphology is a construction of 20 (111) thin plates on the particle surface. The formation mechanism of the pseudo-icosahedral morphology is proposed based on the experimental observation of the morphology evolution and structural investigation. The most important step is the formation of spherical particles containing Cu nanocrystallites capped by PVP molecules. The polycrystalline particles undergo surface recrystallization to form 20 separated (111) plates of Cu and gradually form a pseudo-icosahedral shell followed by an extension of recrystallization from the surface to the core. Throughout the whole process, PVP not only served as a mild reducing agent reducing Cu^{2+} to Cu^+ and to Cu in a multistep process but also functioned as an agglomerating surfactant participating in the crystal growth.

It is demonstrated that, in a thermodynamically controlled growth process of surface crystallization, crystalline shells would naturally choose a morphology as close as possible to a minimum total surface free energy (E_{tot}) by two fundamental approaches, preferentially forming plates with the minimum surface binding energy (E_b) and then achieving a minimum specific surface area (A_s). When there is only one type of facet, e.g., in the cases of the Cu octahedron and icosahedron as we discussed in this work, the particles choose the latter so as to reduce A_s and therefore reduce E_{tot} by about 10%. In general, these two factors are competitive. When plates with the lowest E_b form, the A_s value may increase. When the A_s reduces, the particle may have to exhibit more than one type of facet, and the corresponding E_b may not remain the lowest value. Many polyhedra consist of more than one type of facet to reduce the total specific surface area, A_s, with a cost of increasing E_b. The total surface free energy is $E_{tot} = \sum_{1}^{i} (E_{bi} \times A_{si})$, where "$i$" represents the different types of facets. Consequently, in a thermodynamically controlled crystal growth system, the final polyhedral morphology at an equilibrium state can be predicted, although, in practice, it is very rare to achieve an equilibrium state. The pseudo-icosahedron is not an equilibrium state. A truncated icosahedron can have a lower surface free energy than the icosahedron (Figure S12). Consequently, the formation of the real morphology of pseudo-icosahedron Cu results from a balance between the formation of the (111) facets with the lowest surface binding energy and approaching to the minimum specific surface area.

■ ASSOCIATED CONTENT

ⓢ Supporting Information

The Supporting Information is available free of charge at https://pubs.acs.org/doi/10.1021/acs.cgd.2c00069.

Figure S1, color appearance of the samples; Figure S2, PVP structures; Figure S3, structural model and SEM image of $Cu_4SO_4(OH)_6\cdot H_2O$; Figure S4, EDS spectra of a $Cu_4SO_4(OH)_6\cdot H_2O$ microflake and a Cu_2O/PVP spherulite; Figure S5, the TEM image of nanocrystallites; Figure S6, FTIR and SXES spectra; Figure S7, SEM images and EDS spectra of rough surface spherulites; Figure S8, SEM images of damaged rough surface spherulites; Figure S9, SEM images of Cu/PVP aggregates; Figure S10, SEM images of pseudo-icosahedral particles with thick surface plates and a broken surface. The HRTEM image of an edge of a pseudo-icosahedral particle; Figure S11, FTIR and EDS spectra of the 12 h sample; and Figure S12, model of a truncated icosahedron (PDF)

■ AUTHOR INFORMATION

Corresponding Author

  Wuzong Zhou − *School of Chemistry, University of St Andrews, Fife KY16 9ST, UK;* ⓞ orcid.org/0000-0001-9752-7076; Email: wzhou@st-andrews.ac.uk

Author

  Weihao Sun − *School of Chemistry, University of St Andrews, Fife KY16 9ST, UK*

Complete contact information is available at:
https://pubs.acs.org/10.1021/acs.cgd.2c00069

Notes

The authors declare no competing financial interest.

■ ACKNOWLEDGMENTS

■ REFERENCES

(1) Bravais, A. *Études Crystallographic;* Gauthier-Villars: Paris 1866.

(2) Friedel, M. G. Étudessurla loi de bravais. *Bull. Soc. Fr. Mineral Cristallogr* **1907**, *30*, 326−455.

(3) Donnay, J. D. H.; Harker, D. A new law of crystal morphology extending the law of Bravais. *Am. Mineral.* **1937**, *22*, 446−467.

(4) Hartman, P.; Perdok, W. G. On the relations between structure and morphology of crystals. II. *Acta Crystallogr.* **1955**, *8*, 521−524.

(5) Docherty, R.; Clydesdale, G.; Roberts, K. J.; Bennema, P. Application of Bravais-Friedel-Donnay-Harker, attachment energy and Ising models to predicting and understanding the morphology of molecular crystals. *J. Phys. D: Appl. Phys.* **1991**, *24*, 89−99.

(6) Curie, P. Sur la formation des cristaux et sur les constantes capillaires de leurs différentes faces. *Bull. Soc. Fr. Mineral Cristallogr.* **1885**, *8*, 145−150.

(7) Wulff, G. XXV. Zur frage der geschwindigkeit des wachsthums und der auflösung der krystallflächen. *Z. Kristallogr.* **1901**, *34*, 449−530.

(8) Gao, Y.; Jiang, P.; Song, L.; Wang, J. X.; Liu, L. F.; Liu, D. F.; Xiang, Y. J.; Zhang, Z. X.; Zhao, X. W.; Dou, X. Y.; Luo, S. D.; Zhou, X. Y.; Xie, S. S. Studies on silver nanodecahedrons synthesized by PVP-assisted N,N-dimethylformamide (DMF) reduction. *J. Cryst. Growth* **2006**, *289*, 376−380.

(9) Tsuji, M.; Ogino, M.; Matsuo, R.; Kumagae, H.; Hikino, S.; Kim, T.; Yoon, S. H. Stepwise growth of decahedral and icosahedral silver nanocrystals in DMF. *Cryst. Growth Des.* **2010**, *10*, 296−301.

(10) Ma, X.; Lin, F.; Chen, X.; Jin, C. Unveiling growth pathways of multiply twinned gold nanoparticles by in situ liquid cell transmission electron microscopy. *ACS Nano* **2020**, *14*, 9594−9604.

(11) Seo, D.; Il Yoo, C.; Chung, I. S.; Park, S. M.; Ryu, S.; Song, H. Shape adjustment between multiply twinned and single-crystalline polyhedral gold nanocrystals: decahedra, icosahedra, and truncated tetrahedra. *J. Phys. Chem. C* **2008**, *112*, 2469−2475.

(12) Silly, F.; Castell, M. R. Temperature-dependent stability of supported five-fold twinned copper nanocrystals. *ACS Nano* **2009**, *3*, 901−906.

(13) Vikarchuk, A. A.; Dorogov, M. V. Features of the evolution of the structure and morphology of the surface of icosahedral copper particles in the annealing process. *JETP Lett.* **2013**, *97*, 594−598.

(14) Xu, M.; Zhang, L.; Zhao, F. One-pot aqueous synthesis of icosahedral Au as bifunctional candidates for enhanced glucose electrooxidation and surface-enhanced Raman scattering. *ACS Appl. Mater. Interfaces* **2020**, *12*, 12186−12194.

(15) Ji, G.; Ji, A.; Lu, N.; Cao, Z. Formation and morphology evolution of icosahedral and decahedral silver crystallites from vapor deposition in view of symmetry misfit. *J. Cryst. Growth* **2019**, *518*, 89−94.

(16) Si, R.; Zhang, Y.-W.; You, L.-P.; Yan, C.-H. Self-organized monolayer of nanosized ceria colloids stabilized by poly-(vinylpyrrolidone). *J. Phys. Chem. B* **2006**, *110*, 5994−6000.

(17) Koczkur, K. M.; Mourdikoudis, S.; Polavarapu, L.; Skrabalak, S. E. Polyvinylpyrrolidone (PVP) in nanoparticle synthesis. *Dalton. Trans.* **2015**, *44*, 17883−17905.

(18) Xiong, Y.; Washio, I.; Chen, J.; Cai, H.; Li, Z.-Y.; Xia, Y. Poly(vinyl pyrrolidone): A dual functional reductant and stabilizer for the facile synthesis of noble metal nanoplates in aqueous solutions. *Langmuir* **2006**, *22*, 8563−8570.

(19) Washio, I.; Xiong, Y.; Yin, Y.; Xia, Y. Reduction by the end groups of poly(vinyl pyrrolidone): A new and versatile route to the kinetically controlled synthesis of Ag triangular nanoplates. *Adv. Mater.* **2006**, *18*, 1745−1749.

(20) Lim, B.; Jiang, M.; Tao, J.; Camargo, P. H. C.; Zhu, Y.; Xia, Y. Shape-controlled synthesis of Pd nanocrystals in aqueous solutions. *Adv. Funct. Mater.* **2009**, *19*, 189−200.

(21) Wu, S. T.; Blake, J. I.; Guo, L.; Zhou, W. Z. Naturally occurring and biomimetic synthesized calcite spherulites. *Cryst. Growth Des.* **2020**, *20*, 3537−3545.

(22) Safo, I. A.; Werheid, M.; Dosche, C.; Oezaslan, M. The role of polyvinylpyrrolidone (PVP) as a capping and structure-directing agent in the formation of Pt nanocubes. *Nanoscale Adv.* **2019**, *1*, 3095−3106.

(23) Sudha, V.; Murugadoss, G.; Thangamuthu, R. Structural and morphological tuning of Cu-based metal oxide nanoparticles by a facile chemical method and highly electrochemical sensing of sulphite. *Sci. Rep.* **2021**, *11*, 3413.

(24) Song, Y.-J.; Wang, M.; Zhang, X.-Y.; Wu, J.-Y.; Zhang, T. Investigation on the role of the molecular weight of polyvinyl pyrrolidone in the shape control of high-yield silver nanospheres and nanowires. *Nanoscale Res. Lett.* **2014**, *9*, 17.

(25) Chen, X. T.; Qiao, M. H.; Xie, S. H.; Fan, K. N.; Zhou, W. Z.; He, H. Y. Self-construction of core−shell and hollow zeolite analcime icositetrahedra: A reversed crystal growth process via oriented aggregation of nanocrystallites and recrystallization from surface to core. *J. Am. Chem. Soc.* **2007**, *129*, 13305−13312.

(26) Greer, H.; Wheatley, P. S.; Ashbrook, S. E.; Morris, R. E.; Zhou, W. Z. Early stage reversed crystal growth of zeolite A and its phase transformation to sodalite. *J. Am. Chem. Soc.* **2009**, *131*, 17986−17992.

(27) Zhou, W. Z. Reversed crystal growth. *Crystals* **2019**, *9*, 7.

(28) Lv, T.-T.; Xing, H.-Z.; Yang, H.-M.; Wang, H.-X.; Shi, J.; Cao, J.-P.; Lv, B.-L. Rapid synthesis of Cu_2O hollow spheres at low
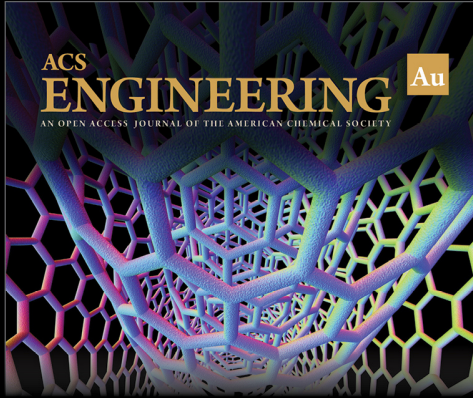
temperature and their catalytic performance for the decomposition of ammonium perchlorate. *CrystEngComm* **2021**, *23*, 7985−7993.

(29) Ritchie, A. W.; Watson, M. I. T.; Turnbull, R.; Lu, Z. Z.; Telfer, M.; Gano, J. E.; Self, K.; Greer, H. F.; Zhou, W. Z. Reversed crystal growth of rhombohedral calcite in the presence of chitosan and gum Arabic. *CrystEngComm* **2013**, *15*, 10266−10271.

(30) Lu, S.-C.; Hsiao, M.-C.; Yorulmaz, M.; Wang, L.-Y.; Yang, P.-Y.; Link, S.; Chang, W.-S.; Tuan, H.-Y. Single-crystalline copper nano-octahedra. *Chem. Mater.* **2015**, *27*, 8185−8188.

(31) Zhang, W.; Liu, Y.; Cao, R.; Li, Z.; Zhang, Y.; Tang, Y.; Fan, K. Synergy between crystal strain and surface energy in morphological evolution of five-fold-twinned silver crystals. *J. Am. Chem. Soc.* **2008**, *130*, 15581−15588.

(32) Bao, S.; Zhang, J.; Jiang, Z.; Zhou, X.; Xie, Z. Understanding the formation of pentagonal cyclic twinned crystal from the solvent dependent assembly of Au nanocrystals into their colloidal crystals. *J. Phys. Chem. Lett.* **2013**, *4*, 3440−3444.